RESEARCH PAPER

Unraveling Multi-Target Interactions of Nilgirianthus ciliatus (Nees) Bremek. Triterpenoids Against Pulmonary Disease via Network Pharmacology, Docking, and Molecular Dynamics.

Pavan Kumar Katukukke[1], Collince Omondi Awere[2], Venkatramanan Varadharajan[3], Manikandan Ramesh[4]*

[1]*PhD scholar, Department of Biotechnology, Science Campus, Alagappa University, Karaikudi, Tamilnadu- 630003, India,*
orcid id- 0000-0003-2170-144X
[2]*PhD scholar, Department of Biotechnology, Science Campus, Alagappa University, Karaikudi, Tamilnadu- 630003, India,*
orcid id- 0000-0002-7763-0997
[3]*Assistant Professor, Department of Biotechnology, PSG College of Technology, Peelamedu, Coimbatore, India,*
orcid id-0000-0002-5608-7737
*[4]*Professor, Department of Biotechnology, PSG College of Technology, Peelamedu, Coimbatore, India,*
orcid id-0000-0002-7969-4935

ABSTRACT

Pulmonary inflammation (PI), pulmonary fibrosis (PF), and lung cancer (LC) manifest a progressive disease continuum driven by chronic immune activation, oxidative stress, and aberrant tissue remodeling. Given the limited effectiveness of single-target therapies in modulating these interlinked pathways, plant-derived multi-target compounds represent a plausible therapeutic option. This study systematically explored the multi-target potential of Nilgirianthus ciliatus (Nees) Bremek (NC). phytoconstituents against pulmonary diseases using integrated network pharmacology, molecular docking, toxicity assessment, and molecular dynamics simulations. A total of 821 NC phytocompounds-related genes and over 22,000 disease-associated genes were mined, revealing 157 common molecular targets. Protein–protein interaction analysis revealed STAT3, SRC, JUN, AKT1, and ESR1 as major hub nodes governing inflammatory and fibrotic signaling. GO and KEGG enrichment displayed significant involvement of oxidative stress responses, cytokine signaling, PI3K–Akt, MAPK, TNF, and IL-17 pathways, which indicates molecular relevance to pulmonary injury and remodeling. Docking analysis revealed outstanding STAT3 binding affinities for triterpenoids like lupeol, β-amyrin, and squalene; in particular, squalene was found to possess good stability and predicted low toxicity (Class V). Molecular Dynamic simulation of the STAT3–squalene complex revealed stable binding, with minimal conformational drift and consistent hydrophobic interaction involving key residues, thus indicating sustained inhibitory potential therein. Collectively, these findings underpin the potential of NC terpenoids—especially squalene to modulate multiple pathogenic targets and axes implicated in pulmonary inflammation, fibrosis, and carcinogenesis. This computational evidence positions NC as a promising candidate for further experimental validation and development of multi-target therapeutics against chronic lung disorders.

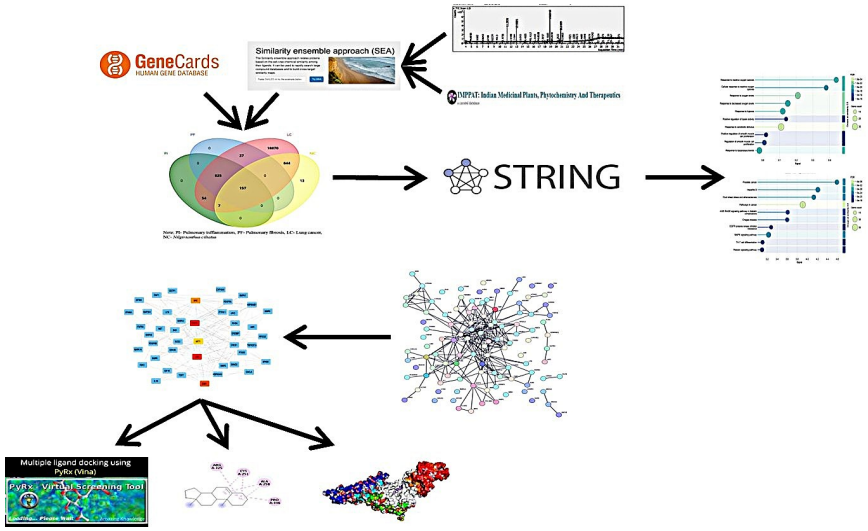

Keywords: Phytoconstituents; Terpenoids; Multi-target therapy; pulmonary disease; Network pharmacology; Molecular docking.

**Author for Correspondence: Manikandan Ramesh*

How to cite this article: Katukukke PK, Awere CO, Varadharajan V, Ramesh M,. Unraveling Multi-Target Interactions of Nilgirianthus ciliatus (Nees) Bremek. Triterpenoids Against Pulmonary Disease via Network Pharmacology, Docking, and Molecular Dynamics...Int J Drug Deliv Technol. 2026;16(2s): 897-908; DOI: 10.25258/ijddt.16. 897-908
Source of support: Nil.
Conflict of interest: None

INTRODUCTION

Pulmonary inflammation (PI), pulmonary fibrosis (PF), and lung cancer (LC) are diseases of the respiratory system with an important global disease burden. The disease initiation is driven by repeated environmental exposures and infectious effect that cause chronic pulmonary inflammation, which activates the transcriptional regulators NF-κB and MAPK, thus eliciting cytokine overexpression, immune cell infiltration, and oxidative stress (Fan et al., 2015; Saleem, 2024; Y. Zhang et al., 2022). Over time, and in the absence of resolution, chronic inflammatory cascades in TGF-β and PI3K-Akt signaling induce fibrotic remodeling that leads to PF (Savin et al., 2022; Wang et al., 2021; Y. Zhou et al., 2024). As PF progresses, an evolving fibrotic remodeling modifies the lung microenvironment, which provides a permissive niche for oncogenic transformation that ultimately increases LC risk (Kinoshita & Goto, 2019; Samarelli et al., 2021; Tzouvelekis et al., 2019, 2022). This continuum of disease burden signals the urgent need for therapeutic interventions that can modify concomitant signaling networks rather than solely targeting individual pathways or phases of disease.

Network pharmacology strategies identified the hub genes MAPK, STAT3, JUN ATK and many more pathway genes as the key regulators of concerted signaling inflammation (Yu et al., 2024), fibrosis (Kasuya et al., 2021; Y. Zhou et al., 2024), and carcinogenesis (Sin et al., 2020; Tran, 2021). Abrogation of such signaling hubs not only increases cellular signals of survival and growth but also causes immune dysregulation, extracellular matrix remodeling, and improper tissue repair mechanisms. Together, these data create a molecular setting that supports chronic inflammation, a fibrotic disease process, and an oncogenic transformation. Modulation of this intricate crosstalk by single-target drugs in combinations is not possible, underscoring the rationale for multi-target therapies that, when taken together, are capable of modulating several key pathways simultaneously.

Medicinal plants are a terminal resource for multitarget agents. *Nilgirianthus ciliatus* (Nees) Bremek. (NC), a vulnerable medicinal shrub endemic to the Western Ghats of India, which belongs to the Acanthaceae family, has been used in traditional medicine for centuries for the management of various ailments, such as inflammation, glandular hypertrophy, and wound healing (Kumar et al., 2025; Rameshkumar et al., 2018; Srinivasan et al., 2024). Phytochemical studies indicate that the plant has terpenoids, flavonoids, phenolics icluding squalene, lupeol, stigmasterol in its composition, some of these have antioxidant, anti-inflammatory, and cytoprotective activities (Amarowicz, 2009; Bidooki et al., 2024; Cárdeno et al., 2015). Among these phytochemicals, squalene serves as a precursor for all other phytosterols; its oxidation through various biosynthetic pathways leads to the formation of distinct phytosterols. The plant has yet to be fully characterized for its pharmacological benefits in complex pulmonary diseases.

Systems biology and computational methods have become potent means of filling this gap. In most studies, disease-related genes, compound-target relationships, and protein-protein networks are combined to detect hub genes and pathways (Mohanty et al., 2024; Rout et al., 2024; Shi et al., 2025). Enrichment tools like Gene Ontology (GO) and Kyoto Encyclopedia of Genes and Genomes (KEGG) draw out biological process and signaling cascade context, whereas molecular docking demonstrates how phytochemicals can bind and modulate key proteins (Gao et al., 2022; Li et al., 2021; Zhang et al., 2020). In addition, toxicology profiling guarantees that lead compounds have good pharmacokinetic properties, increasing their translational value (Balani et al., 2005; Chung et al., 2015; Tarbit & Berman, 1998).

Where molecular docking represents the static conformation of the binding structure, MD simulations complement these by enabling the study of biomolecular interactions under dynamic and physiologically relevant conditions. Unlike pure docking, which is a simple snapshot of the binding conformation, MD simulations reflect time-dependent fluctuations and flexibility of proteins and solvent that influence the stability of their complexes over time (Karplus & McCammon, 2002). Moreover, by tracking parameters like RMSD, RMSF, and solvent accessibility, MD is able to assess the stability of the ligand in its binding pose or its dislocation within the active site during simulation events (Durrant & McCammon, 2011). In addition, MD enables the visualization of induced fit adjustments and new stabilizing interactions that are not observable from static models, increasing accuracy in predictions of ligand compatibility and permeability (Hollingsworth & Dror, 2018). The integration of these two techniques, therefore, certainly offers one a more comprehensive and reliable perspective on how phytocompounds interact at the molecular level with pulmonary disease targets. Cumulatively, these approaches form a systems-based rationale for appreciating how plant-derived compounds can function as multi-target therapeutic agents.

Within this context, NC is a timely and promising lead for investigation. Through the combination of ethnomedicinal knowledge and systems biology, it is potentially a source of new plant-derived interventions for PI, PF, and LC with sustainable solutions at a time when the chronic burden of lung disease globally keeps increasing while treatment options remain limited. To our knowledge, this is the first detailed study to associate the phytochemicals of NC in relation to the genetic pathways and signaling networks

responsible for pulmonary fibrosis, inflammation, and lung cancer, with its newly recognized therapeutic potential as a multi-target drug.

2.0 Materials and Methods

2.1 Identification of Disease-Related Genes

Disease-linked protein-coding genes related to pulmonary inflammation, pulmonary fibrosis and lung cancer were downloaded from the GeneCards database (https://www.genecards.org/). Genes annotated as protein coding only were considered for downstream analysis to guarantee functional significance in subsequent pathway research.

2.2 Identification of Compound-Related Target Genes

Phytoconstituents of NC were chosen through literature mining, GC–MS profiling (Kumar et al, 2025), and accessible phytochemical databases- Indian Medicinal Plants, Phytochemistry and Therapeutics (IMMPAT). Target genes for the reported compounds were predicted through the Similarity Ensemble Approach (http://sea.bkslab.org). Genes related to human beings were only considered for downstream analysis.

2.3 Integration and Identification of Common Targets

To identify the therapeutic significance of NC phytoconstituents in pulmonary diseases, the compound-related gene set was contrasted with disease-related gene sets. Overlaps for genes were calculated employing Venny 2.0 (https://bioinfogp.cnb.csic.es/tools/venny).

2.4 Connecting Proteins in PPI Networks

Common protein-coding genes were uploaded to the STRING database (https://string-db.org/), and the goal was to build a protein–protein interaction (PPI) network on-line. A maximum high-confidence score cutoff of 0.8 was applied, and nodes without any connections were dropped to make network organization more informative. The PPI network was then captured.

2.5 Gene Ontology (GO) and KEGG Pathway Enrichment Analysis

Functional annotation analysis for the target genes in common was performed in STRING using its internal GO and KEGG (Kyoto Encyclopedia of Genes and Genomes) modules. The GO enrichment analysis was performed as a function of Biological Process (BP). In parallel, a KEGG enrichment analysis was performed to identify signaling cascades that were significantly associated with the common targets within 157. The significance for the enrichment analyses was defined as FDR adjusted p-value < 0.05. Connecting Proteins in PPI Networks.

2.6 Visualization and Analysis of Hub Genes

The PPI network from STRING was exported as tab-separated and loaded into Cytoscape v3.10.3 for extensive visualization and topological analysis. Nodes of the network were colored and sized based on their degree values to emphasize highly interacting proteins.

Using the CytoHubba, Cytoscape plugin, was used inidentifying hub genes. Five centrality was employed i.e,: Degree, Closeness, Betweenness, Maximal Clique Centrality (MCC), and Edge Percolated Component (EPC), to evaluate and order the nodes in the networks. The highest-ranking five nodes were designated hub genes and are presumed to be the key regulatory nodes in the compound therapeutic action of NC on pulmonary ailments. A sub network of these top five hub genes and their immediate interacting partners was extracted to enable convenient visualization of significant interactions. All figures were saved from Cytoscape in high-resolution formats.

2.7 Molecular Docking Analysis

The five leading hub genes obtained from CytoHubba were chosen as molecular targets to be subjected to docking analysis. Matching three-dimensional protein structures were downloaded from the Protein Data Bank (PDB-https://www.rcsb.org/) in PDB format and selected on the basis of high resolution and completeness. Proteins were prepared before docking by deleting water molecules, adding polar hydrogens, and assigning Kollman charges using Discovery studio. 30 phytocompounds reported for NC were employed as ligands. The structures of the ligands were retrieved from the PubChem database (https://pubchem.ncbi.nlm.nih.gov/) in 3D SDF format and converted to PDBQT format using Open Babel Ligand energy minimization was performed prior to docking. Molecular docking simulations were carried out on PyRx 0.8, utilizing the Vina engine. Docking was done with an exhaustiveness value of 8, and grid box size defined to span the whole active site of all protein targets (Binding site axes retrieved from PDB through Discovery studio). In each ligand–protein combination, multiple poses of binding were generated, and the lowest binding free energy (kcal/mol) conformation was chosen as the best-binding mode. The binding affinities of all ligand–protein interactions were summarized, and the most negative binding energy against each hub protein was determined as potential key modulators of pulmonary disease-related pathways.

2.8 Post-Docking Visualization and Interaction Analysis

30 compounds of NC were docked against all the 5 hub proteins and compounds achieving low docking scores were chosen for subsequent evaluation. Docked complexes were viewed and inspected using BIOVIA Discovery Studio Visualizer 2024 to determine the type of ligand–protein interaction, i.e., hydrogen bonds, hydrophobic interaction, van der Waals forces, and π–π stacking. Important interacting residues in the active sites were overlayed to estimate the stability and selectivity of compound binding. To confirm the docking conformations and to demonstrate three-dimensional interactions, the chosen protein–ligand complexes were also explored using PyMOL. PyMOL was utilized to create high-resolution molecular graphics displaying binding pockets, hydrogen bonding distances, and ligand orientation within the receptor cavity. The interaction profiles of each compound with the hub proteins were contrasted to determine recurring amino acid residues

and conserved modes of binding. These findings were utilized to rank lead phytocompounds based on robust and reproducible binding affinities at multiple hub genes.

2.9 Toxicity Predictor

The toxicity profiles of the top STAT3-binding phytocompounds were evaluated using the ProTox-3.0 web server (https://tox.charite.de/protox3/). For each compound name, it was manually inputted directly to the toxicity predicting query interface. ProTox-3.0 uses sophisticated machine learning models as well as molecular similarity-driven strategies to predict compound toxicity at several biological endpoints. The following predicted parameters were calculated: the median lethal dose (LD, mg/kg), toxicity class (I–VI) according to the Globally Harmonized System (GHS), as well as toxicity endpoints for selected effects, including hepatotoxicity, carcinogenicity, immunotoxicity, mutagenicity, and cytotoxicity. It further offered estimations for possible toxicity targets as well as mechanistic routes, allowing for a global *in silico* evaluation of the safety as well as drug-likeness of the compounds. The compound with very low toxicity was selected for further dynamics study.

2.10 Molecular Dynamics (MD) Simulations

The protein-ligand complex was done based on [6NJS-STAT3/ Squalene]. PH 7.0 was protonated with PROPKA and missing residues with MODELLER. amber ff14SB protein parameters were obtained and ligand parameters provided by GAFF2 with AM1-BCC charges provided using Antechamber. The complex was dissolved in a cubic box full of TIP3P water that expelled 10 A of the solute and neutralized to 0.15 M NaCl. The steepest descent was minimized until the force was below 1000 kJmol-1nm-1. Equilibration was done in systems under the NVT (0.5ns) and NPT (1ns) ensembles with positional restraints (1000 kJmol-1nm-2 of heavy atoms) under the V-rescale thermostat (300K) and Parrinello-Rahman barostat (1bar). The simulation MD Production MD was simulated using a 2-fs timestep, LINCS constraints, PME electrostatics (1.2 nm cutoff) and a Verlet cutoff scheme, and 100 ns of simulation time. SCHRODINGER tools and MD Analysis were used to process trajectories and analyze them on a structural stability scale (Root Mean Square Deviation-RMSD, Root Mean Square Fluctuation-RMSF), the properties of the ligands (Radius of Gyration- rGyr, Solvent Accessible Surface Area-SASA, Polar Surface Area-PSA), the torsional distributions, hydrogen bonds and protein-ligand contacts. Three replicates were done working independently to guarantee reproducibility. Representative input scripts and parameter files are on request.

3.0 Results and Discussion

3.1 Data mining-based identification of shared molecular targets among NC and pulmonary diseases

To elucidate the likely molecular mechanisms of the therapeutic efficacy of NC bioactive compounds on pulmonary conditions, the data mining approach was applied to mobilize compound- and disease-associated gene information. A total of 1043 protein-coding genes for pulmonary inflammation (PI), 1009 genes for pulmonary fibrosis (PF), and 20,584 genes for lung cancer (LC) were retrieved exclusively from the GeneCards database. At the same time, 821 target genes for the identified phytocompounds of NC were retrieved from the Similarity Ensemble Approach (SEA) database and from scientific literature, using human protein-coding genes only for ensuring biological and therapeutic significance.

The intersection of these datasets was depicted in the form of a Venn diagram (Fig 1), revealing 157 common genes present in NC, PI, PF, and LC that constituted the potential common molecular targets of NC. These targets in their functioning have associations with key biological processes such as inflammation, regulation of oxidative stress, apoptosis, and cell proliferation, which form the core of the pathogenesis of pulmonary inflammation, fibrosis, and carcinogenesis.

These findings align with established links between shared inflammatory–fibrotic–oncogenic molecular networks and support the use of common gene signatures to reveal multi-target plant-based therapeutic mechanisms. The 157 common targets were subsequently used for protein–protein interaction (PPI) network building in STRING and for functional enrichment (GO and KEGG) to uncover their regulatory relevance

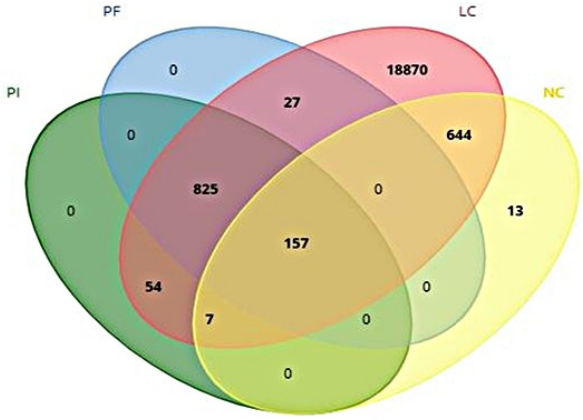

Fig 1: Venn Diagram showing intersection of genes between Pulmonary inflammation (PI), pulmonary Fibrosis (PF), lung cancer (LC) and *N. ciliatus* (NC)

3.2 Protein–Protein interaction analysis

The intersection target genes acquired from the interaction between bioactive molecules of NC and their related genes to pulmonary diseases were further subjected to the STRING database to analyze hypothetical PPIs. The PPI network (Fig. 2A) constituted a densely interconnected cluster of nodes (proteins) and edges (inferred functional associations). The higher clustering coefficient and tighter network connectivity indicated that the unveiled targets are functionally related and possibly synergistically control cell processes relevant to inflammation, fibrosis, and tumorigenesis.

The STRING network that was generated was uploaded to Cytoscape (v3.9.1), where the nodes were evaluated for degree, betweenness, and closeness centrality using CytoHubba. The results indicated STAT3, SRC, JUN, AKT1, and ESR1 as the top five hub genes (Fig. 2B). The hub genes represented the highest number of interactions,

and because of their interactions with signaling proteins, they provide a central location in the PPI network and suggest these genes may be important for signal transduction and transcription regulation.

These observations correspond well with known roles of these genes. STAT3 is widely recognized as a pathological convergence node for chronic inflammation and pulmonary fibrosis, where chronic IL-6/JAK-driven STAT3 activation promotes pro-survival and pro-fibrotic transcription ((Tieyuan et al., 2022). JUN functions downstream of MAPK signals responsive to stress and cytokines, SRC and AKT1 act as upstream kinases controlling PI3K–Akt and oxidative stress responses, and ESR1 regulates gene expression related to immune and fibrotic signaling. Their identification as hubs therefore places NC compounds at central signaling intersections relevant to inflammatory and fibrotic modulation

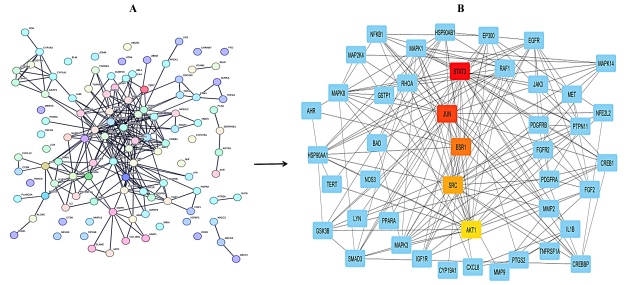

Fig 2: (A) Protien-Protein interaction network by string software and (B) Top 5 Hub protiens obtained by cytoscape (Marked in Shades of Yellow, Red and orange)

3.3 GO and KEGG Enrichment Analysis

The Gene Ontology (GO) enrichment analysis (Fig. 3A) of the common target genes identified between NC bioactive compounds and pulmonary disease–associated genes revealed significant enrichment in biological processes crucial in inflammation and tissue injury regulation. Prominent enriched GO terms included response to oxidative stress, regulation of apoptotic signaling pathways, cytokine-mediated signaling, and cellular response to chemical stress. These GO categories collectively point to the potential roles of the compounds in restoring redox homeostasis and modulating immune–inflammatory cascades. The enrichment of oxidative stress–related terms underscore the phytoconstituents' possible antioxidant capacity, which can mitigate reactive oxygen species–driven epithelial injury.

The KEGG pathway enrichment analysis (Fig. 3B) revealed enrichment of the common target genes mainly in PI3K–Akt, MAPK, TNF, and IL-17 signaling pathways, which are key regulatory centers in the processes of inflammation, oxidative stress response, and fibrotic remodeling. Enrichment of the PI3K–Akt pathway hints at cell survival promotion and apoptosis attenuation, while MAPK cascade modulation indicates influence over inflammatory gene expression and stress-activated kinase signaling. Inclusion of the TNF and IL-17 pathways signifies potential effects on cytokine-driven inflammation and immune cell recruitment.

These patterns coincide with known mechanistic associations between oxidative stress, inflammatory cytokine signaling, and fibrotic remodeling (Tieyuan et al., 2022)demonstrating that the enriched targets lie within hallmark pathways of lung injury. Overall, the GO and KEGG enrichment results present that NC phytoconstituents exert multi-target and multi-pathway modes of action through oxidative stress regulation, apoptosis modulation, cytokine signaling, and survival pathway influence.

3.4 Molecular docking of top-ranked hub protein STAT3 with phytocompounds of NC

For screening of compound–target interactions predicted from network pharmacology, molecular docking was performed using PyRx against the highest scored hub protein STAT3 (PDB ID: 6NJS), which is key in pulmonary inflammation through cytokine signaling regulation and transcription activation. 30 phytocompounds of NC were screened, and the top 5 best binding affinity compounds (Min et al., 2019)β-amyrin, lupeol, campesterol, stigmasterol, and squalene were selected for interaction analyses.

The findings revealed that all compounds had stable binding affinities ranging from –6.4 to –7.6 kcal/mol, reflecting moderate to strong interactions with the STAT3 active site. Lupeol had the highest binding affinity (–7.6 kcal/mol), forming hydrophobic interactions with ALA505, ILE522, LEU525, VAL537, and TRP501. β-amyrin showed –7.4 kcal/mol with interactions involving ALA250, CYS251, and ARG325. Campesterol and stigmasterol showed –7.2 and –7.0 kcal/mol, respectively, forming alkyl interactions with ALA250, CYS251, ARG325, and PRO336. Squalene had –6.4 kcal/mol with hydrophobic contacts involving LYS370, LEU438, LYS488, VAL490, and HIS457 (Fig 4)

These docking patterns agree with earlier work reporting that lupeol inhibits EGFR/STAT3 phosphorylation, nuclear translocation, and downstream transcriptional activation in lung cancer cells, suppressing proliferation (Min et al., 2019). The overlapping hydrophobic pockets occupied by phytoconstituents around STAT3's catalytic domain suggest potential inhibition of STAT3 activation by stabilizing its inactive state, consistent with the pathological significance of STAT3 in pulmonary fibrosis and inflammation (Gao et al., 2022; Pedroza et al., 2016)

3.5 Toxicity analysis

The bioactivity radar plot of lupeol indicated strong predicted interactions with metabolic enzymes (CYP1A2, CYP2C19, CYP3A4) and with adrenergic, dopaminergic, and serotonergic receptors. Toxicity prediction of Class IV (LD50 ≈ 1000 mg/kg) confirmed low acute oral toxicity and favorable safety. β-Amyrin showed similar broad interactions with CYP450 isoforms and nuclear hormone receptor signaling, along with Class IV toxicity classification. Campesterol exhibited strong predicted activity toward CYP1A2, CYP2D6, and CYP3A4 but showed medium toxicity (ClassIII; LD50 ≈ 500mg/kg) and mutagenic or cytotoxic alerts. Stigmasterol displayed moderate interactions and Class IV toxicity, indicating tolerability. Squalene demonstrated the broadest bioactivity profile with predicted interactions across multiple receptor

families and CYP enzymes, accompanied by very low toxicity (Class V; LD50 > 2000 mg/kg) and no mutagenic or carcinogenic alerts (Fig 5).

These toxicity and ADME characteristics agree with existing reports describing similar anti-inflammatory, antioxidant, hepatoprotective, and metabolic profiles for Lupeol (Banu, 2024) , β-amyrin (Tzouvelekis et al., 2019), campesterol and sterol derivatives (Sanders et al., 2000), and squalene (Relas et al., 2001). Overall, squalene, β-amyrin, and lupeol emerge as promising lead candidates for pharmacological development. However, due to its less toxicity (Toxicity level- V) and high pharmacological relevance squalene was selected for further Molecular simulation dynamics with top HUB protein-STAT3

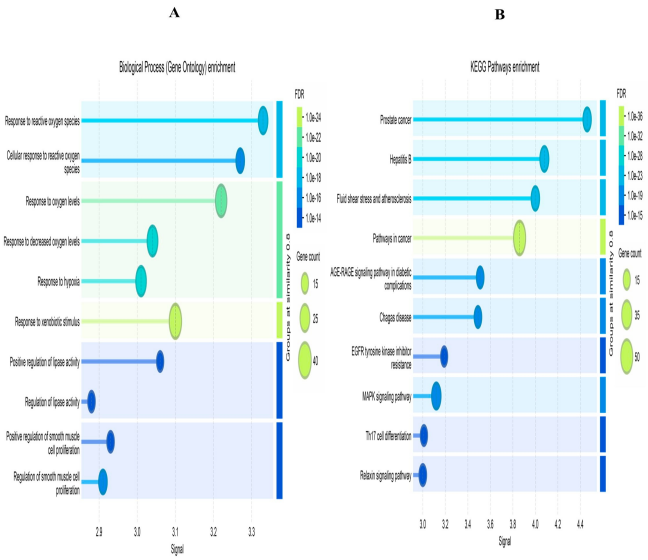

Fig 3: GO and KEGG enrichment of common target genes between NC compounds and pulmonary diseases. (A) GO-BP bubble plot showing enrichment in oxidative stress, cytokine signaling, and apoptosis. (B) KEGG bubble plot highlighting PI3K–Akt, MAPK, TNF, and IL-17 pathways. Bubble size reflects gene count; color shows FDR significance in TNF, and IL-17 pathways

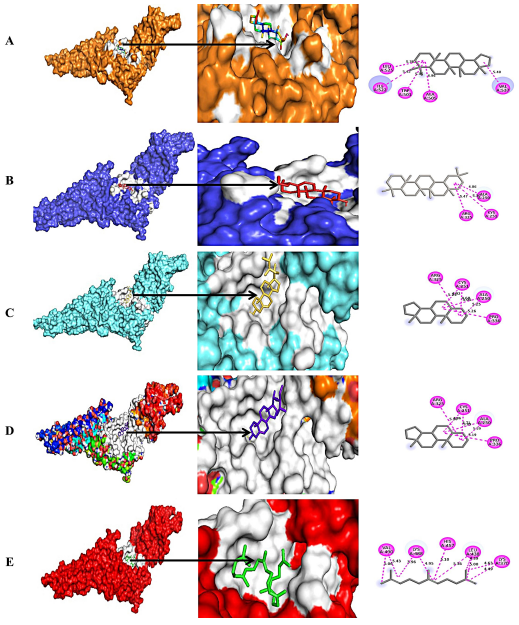

Fig 4: 3D and 2D interaction view of Stat-3 Protein with ligands (A) Lupeol (B) β-amyrin (C) Campesterol (D) Stigmasterol (E) Squalene

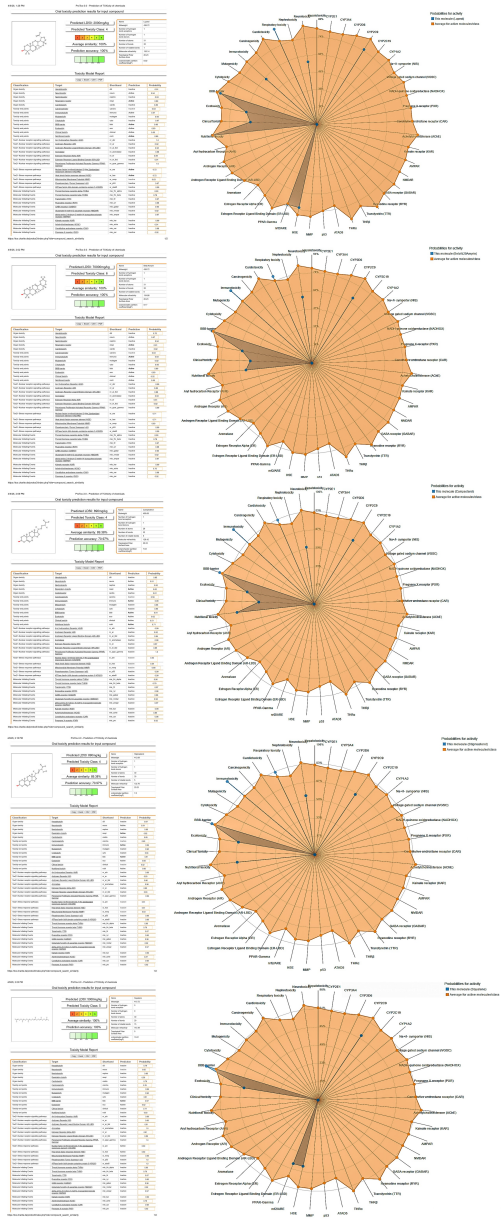

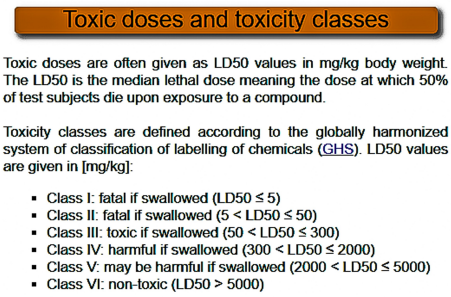

Fig 5: Toxicity report and Toxicity radar report of top five compounds based on binding affinity (A) Lupeol (B) β-amyrin (C) Campesterol (D) Stigmasterol (E) Squalene

3.6 Ligand Properties during MD Simulation

The ligand (Squalene) RMSD was not found to drift continuously but instead had moderate variations in which the binding orientation of the ligand in the protein (STAT3) active site remained constant, with local changes presumably found in an aqueous and flexible environment (Fig. 6). This is an expected behavior of well-retained ligands in MD simulations, where positional changes are indicative of adaptive binding and not destabilization (Durrant & McCammon, 2011) . The radius of gyration (rGyr) did not change significantly with time, indicating that the ligand did not unfold or experience a significant conformational collapse. A consistent rGyr value is normally an indication that the internal geometry of the ligand is structurally stable in dynamic conditions (Karplus & McCammo, 2002). There was no evidence of intramolecular hydrogen bonds during the simulation process, meaning that the ligand is not using internal hydrogen bonding networks to stabilize its conformation. Rather, its stability would probably be due to its interaction with the neighboring protein residues or solvent. The MolSA and SASA values were slightly dynamic, which is typical of the normal solvent exposure dynamics as the ligand scouts the microstates inside the binding pocket. This is consistent with what ligands are expected to do in partially buried binding sites, in which they are periodically exposed to solvent as local rearrangements take place (Cournia et al., 2020). The PSA was also held constantly during the simulation that the polar distribution of regions did not change significantly with time. Constant PSA values are typically associated with constant hydrogen-bonding potential, and this allows one to interpret that the ligand did not experience significant conformational re-orientation but instead, it was structurally intact (Ertl et al., 2000).

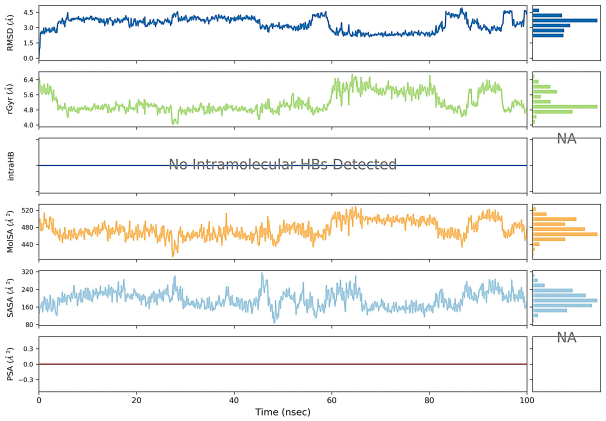

Fig 6: The time-evolution and distribution of key ligand properties over a 100-ns MD simulation, including RMSD, radius of gyration, molecular surface area (MolSA), solvent accessible surface area (SASA), and polar surface area (PSA)

3.7 Root Mean Square RMSD Analysis

The protein RMSD showed an early rise at the initial period of about 10-15 ns that represent the equilibration process where the system assumed the starting conformation. The protein stabilized at RMSD values of 3.0 to 4.0 A after this stage (Fig 7A), which meant that the protein had a stable overall fold with moderate, anticipated variations commonly seen in solvated biomolecular simulations (Hollingsworth & Dror, 2018). Though there were small transient spikes, no long-term drift was seen, indicating that the protein reached a dynamic equilibrium without experiencing large scale conformational rearrangements. Likewise, the ligand RMSD displayed an initial readjustment of the position and stabilization with a range of 5.5 to 7.0 A. Although they are larger than the protein RMSD,
they are comparable to the ligands with internal flexibility or with multiple microstates in case RMSD
is measured after the complex has been aligned to the protein backbone (Durrant & McCammon, 2011). Notably, the ligand RMSD did not experience continuous growth throughout the simulation, and the ligand was retained in the pocket and only experienced local positional changes or rotational freedom and not unbinding events. The finding of no significant drift implies a constant binding interaction over the course of the simulation which is also consistent with behavior during well-retained ligands in MD simulations (Cournia et al., 2020).

3.8 RMSF analysis

The RMSF profile showed that the N-terminal region (residues 1-50) has a very sharp fluctuation, with values greater than 6.0 A (Fig 7B), which is very likely to be a highly flexible or partially disordered region of protein termini because of the lack of secondary structure and extensive solvent exposure (Henzler-Wildman & Kern, 2007). There were moderate changes in residues 50-200 (0.8-1.5 A), which is in agreement with more organized secondary structures like a-helices and b-strands. Flexible loop regions are localized peaks in this segment and often are more mobile than the protein core. The maxima of the fluctuations (0.6-1.2 A) were the lowest, and it was observed in the central region (residues 200-450), which indicates a well-packed and structurally stable domain, which is the core architecture of the protein as expected of globular proteins where interior residues are constrained by large numbers of non-covalent interactions (Bhattacharyya et al., 2015; Janin et al., 2008; Vishveshwara et al., 2009). At the C-terminal end (residues 450-520), there was again an increase in fluctuations to around 3-4 A, which is indicative of terminal flexibility as at the N-terminus. It is interesting to note that residues pointed out in the RMSF plot, which presumably are functional or ligand-binding residues, exhibited moderate yet controlled flexibility, which can be used to support the idea that functional sites typically demand adaptive movement to enable ligand identification, binding, and conformational adjustment (Frauenfelder et al., 2001). Flexibility of the protein is distributed in such a way that there is a dynamic structure with a rigid structural core and flexible strategic termini and loop motifs. This kind of compromise in rigidity and local mobility is typical of proteins that experience minor changes in conformation in response to ligand binding or catalytic activity (Henzler-Wildman & Kern, 2007).

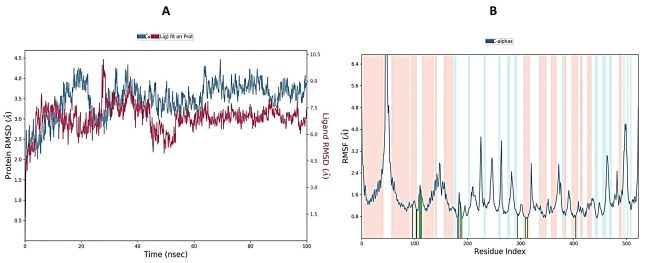

Fig 7: (A) Time-dependent RMSD profiles of the protein backbone and ligand (ligand fitted on protein) over a 100-ns MD simulation. (B) RMSF plot of Cα atoms across all residues, highlighting flexible loop regions (shaded) and relatively stable secondary-structure segments

3.9 Ligand Torsional Stability Test (100 ns MD)

The distributions of torsion angles in the form of combined polar scatter plots and histogram profiles indicate that most of the rotatable bonds sampled well-defined conformational regions throughout the 100 ns MD trajectory (Fig. 9). Several torsions exhibit unimodal distributions closely concentrated around preferred angular values (approximately ±60°, ±90°, and 180°), whereas others display bimodal or trimodal profiles, reflecting reversible transitions between energetically favored conformers. This behavior is typical of ligands that maintain a predominantly static bound conformation within a protein binding pocket while retaining limited internal flexibility necessary for adaptive interactions (Mobley & Dill, 2009).

The histograms of selected torsions show narrow peaks centered around specific dihedral angles, suggesting restricted rotational freedom imposed by steric constraints, intramolecular stabilization, or persistent protein–ligand contacts. These constrained torsional motions likely arise from substituent groups forming stable interactions with key binding-site residues, thereby stabilizing the ligand in a low-energy binding pose (Bissantz et al., 2010). Conversely, torsions characterized by broader or multimodal distributions indicate controlled conformational sampling, corresponding to microstate transitions within energetically accessible rotameric wells. Such low-energy rotations about single bonds are consistent with dynamic adaptability of the ligand inside the binding pocket and contribute favorably to enthalpic and entropic components of binding (Limongelli, 2020).

The polar scatter plots further demonstrate that torsional sampling is not uniformly distributed but instead clustered within energetically favorable regions of the rotameric potential energy surface. Importantly, no torsion exhibits excessively broad or random distributions spanning the full −180° to +180° range, indicating the absence of high-energy or non-physical conformations during the 100 ns simulation. This alignment between sampled conformations and expected torsional energetics suggests that the ligand remains structurally stable, maintaining its overall topology while sampling energetically favorable conformational microstates conducive to productive protein–ligand recognition (Cournia et al., 2020)

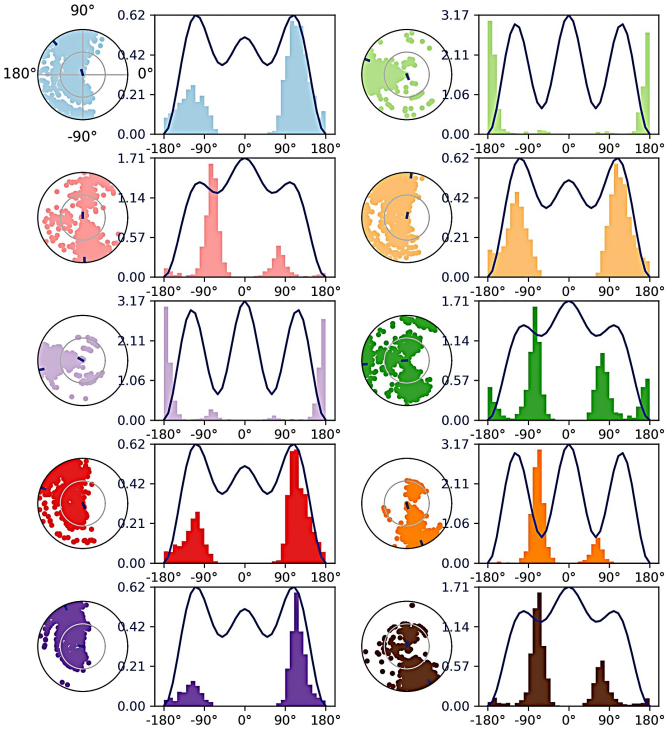

Fig. 8: Ligand Torsional Angle Distribution During MD Simulation.

Polar scatter plots and corresponding histogram distributions of ligand rotatable bonds obtained from Desmond MD simulation. The clustering of torsion angles around specific values indicates energetically favorable conformations and restricted rotational freedom within the binding pocket, reflecting stable ligand accommodation throughout the trajectory.

3.10 Protein–Ligand Contact Histogram Analysis

Several residues showed significantly large interaction fractions, which suggest that contacts were persistent and repeated, and that these contacts play a role in keeping the binding affinity (Fig. 9). One of them, the interaction frequency of PRO336 was the highest, which indicates that the protein takes a central position in anchoring the ligand, which could be achieved through hydrophobic packing due to proline-rich

microenvironment constraints of conformational freedom and tight ligand-binding (Kool et al., 2011; Tuffery & Derreumaux, 2012). Other residues which had a significant number of interactions were ALA250,

PRO256, ILE258, TRP474 and ILE569, which play a role by providing nonpolar contacts that stabilize the hydrophobic core of the binding pocket. The high contact energies of hydrophobic residues are also in line with the dominant van der Waals and dispersion forces in ligand binding, especially in deep or partially blocked binding pockets in which solvent exclusion exaggerates the forces (Bissantz et al., 2010). Weaker binding with such residues as CYS251, LEU260, CYS328, and LEU459 also confirm that the ligand undergoes both peripheral and core interactions, which confirms a multi-residue binding mode, not a single dominant hotspot binding mode. The presence

of tryptophan residues (TRP243, TRP474) in the interacting residues is indicative that there is a further stabilization by the p-p or p-alkyl interactions, which are typically involved in the enhancement of the affinity of the ligand and the control of the orientation (Dougherty, 2013). The general pattern of contacts with hydrophobic and aromatic residues predominant indicates that the ligand binds by nonpolar interactions, which is a typical property of ligands presented by internal or transmembrane-like binding loops where a nonpolar complementarity is used to recognize ligands (Jakowiecki et al., 2020; H.-X. Zhou & Pang, 2018)).

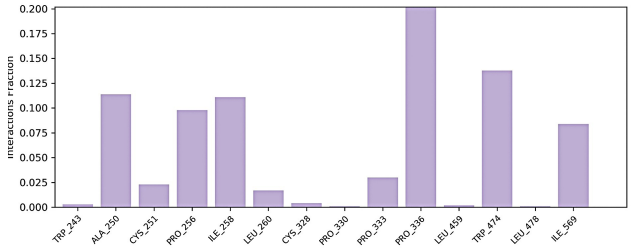

Fig 9: Interaction Fraction of Key Protein Residues with the Ligand. The bar plot illustrates the fraction of simulation time during which specific protein residues formed interactions with the ligand. Higher interaction fractions (e.g., PRO336, TRP474, ALA250) indicate residues that contribute most consistently to ligand binding stability throughout the MD trajectory

3.11 Protein–Ligand Contact Timeline Analysis

The overall contact trace indicated that there were oscillations between one and six simultaneous contacts, no significant dissociation intervals, and exhibited sustained ligand contact and well-maintained binding orientation throughout the trace. Contact mapping based on residue revealed the prevalence of hydrophobic and aromatic residues, especially PRO336, ILE258, LEU260, PRO256 and TRP474 that showed many interaction events scattered around the entire period of the simulation (Fig. 10). This high frequency of contact between proline residues and leucine residues indicates that hydrophobic packing and steric complementarity are significant factors in ligand stabilization and such interactions have been previously recognized as important forces in stabilization of drug-receptor complexes (Bissantz et al., 2010). The continuity of TRP243 and TRP474 further suggests stabilization due to π- stacking or π -alkyl interactions, which are known to substantially increase the binding affinity and orientational specificity of hydrophobic cavities (Dougherty, 2013). Interestingly, the residues like CYS251, CYS328, PRO330, and LEU459 were intermittent, yet repeated in nature, and they are involved in a multi-residue binding mechanism whereby the core and the peripheral interactions are necessary to ensure overall stability. The heterogeneity of the contact intensities, such as single and transient contacts, and broader regions of high-frequency contacts, indicates a flexible binding mode that provides local flexibility and maintains global stability. This is common with ligands that are bound in well-organized hydrophobic pockets, where non-disruptive but dynamic micro-motions further optimize enthalpic and entropic binding energy (Kool et al., 2011; Tuffery & Derreumaux, 2012). The lack of all the interacting residues to be in contact-free regions supports that the ligand is deeply entrenched in the binding pocket and this results support stability trends found in the RMSD and RMSF analyses. In general, the PL contact timeline shows that the ligand has a strong and stable network of interactions during the simulation, which suggests a stable and energetically advantageous binding scheme (Jakowiecki et al., 2020; H.-X. Zhou & Pang, 2018).

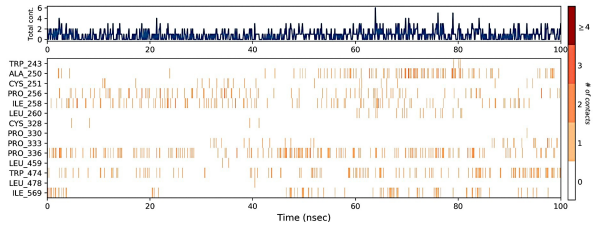

Fig 10: Protein–Ligand Contact Timeline During MD Simulation. The figure shows the total number of proteins–ligand contacts over the 100-ns MD simulation (top panel) and the time-resolved contact map for individual interacting residues (bottom panel). The color intensity represents the number of contacts formed at each time point, highlighting residues that maintain frequent or persistent interactions with the ligand throughout the trajectory

4.0 Conclusion

This study combined data mining, network pharmacology, molecular docking, toxicity prediction, and MD simulation to determine the therapeutic potential of *N.ciliatus* phytocompounds against pulmonary inflammation, fibrosis, and lung cancer. In all, 157 common targets were found, of which STAT3, SRC, JUN, AKT1, and ESR1 were the major regulatory hubs. Squalene, lupeol, and β-amyrin are promising candidates according to in silico docking and ADME–toxicity analyses, given their demonstrated high binding affinity and superior safety profile. From among these, squalene had been selected with the highest pharmacological relevance for MD simulation based on its well-established anti-inflammatory and antioxidant activities, high biological demand, and low predicted toxicity in Class V. MD results confirmed stable binding, with a consistent ligand conformation and sustained interactions with key residues, supporting its suitability as a potential lead molecule. Overall, the findings mechanistically support the therapeutic promise of *N. ciliatus* phytoconstituents and establish squalene as a strong candidate for further experimental validation in pulmonary disease models

Data availability

The authors confirm that the data supporting the findings of this study are made available on request.

Funding sources

This research did not receive any specific grant from funding agencies in the public, commercial, or not-for-profit sectors.

Conflict of interest

The authors declare no conflict of interest.

Acknowledgments

All the authors greatly acknowledge RUSA 2.0 [F.24-51/2014 - U, Policy (TN Multi-Gen), Dept of Edn, GOI]. All the authors sincerely thank the Karnataka Forest Department and Dr. Dinesh Kumar Y. K., Deputy

Conservator of Forests, Mangalore Division, Mangalore, Karnataka for extending their help in plant collection

REFERENCE

1. Amarowicz R. Squalene: A natural antioxidant? Eur J Lipid Sci Technol. 2009;111(5):411–412. doi:10.1002/ejlt.200900102
2. Balani SK, Miwa GT, Gan LS, Wu JT, Lee FW. Strategy of utilizing in vitro and in vivo ADME tools for lead optimization and drug candidate selection. Curr Top Med Chem. 2005;5(11):1033–1038. doi:10.2174/156802605774297038
3. Banu Z. Therapeutic promise of lupeol: A comprehensive review of its pharmacological potential. Ann Phytomed. 2024;13(2). doi:10.54085/ap.2024.13.2.7
4. Bhattacharyya M, Ghosh S, Vishveshwara S. Protein structure and function: Looking through the network of side-chain interactions. Curr Protein Pept Sci. 2015;17(1):4–25. doi:10.2174/1389203716666150923105727
5. Bidooki SH, Quero J, Sánchez-Marco J, Herrero-Continente T, Marmol I, Lasheras R, et al. Squalene in nanoparticles improves antiproliferative effect on human colon carcinoma cells through apoptosis by disturbances in redox balance. Int J Mol Sci. 2024;25(23):13048. doi:10.3390/ijms252313048
6. Bissantz C, Kuhn B, Stahl M. A medicinal chemist's guide to molecular interactions. J Med Chem. 2010;53(14):5061–5084. doi:10.1021/jm100112j
7. Cárdeno A, Aparicio-Soto M, Montserrat-de la Paz S, Bermúdez B, Muriana FJ, Alarcón-de-la-Lastra C. Squalene targets pro- and anti-inflammatory mediators and pathways to modulate over-activation of neutrophils, monocytes and macrophages. J Funct Foods. 2015;14:779–790. doi:10.1016/j.jff.2015.03.009
8. Chung TD, Terry DB, Smith LH. In vitro and in vivo assessment of ADME and PK properties during lead selection and lead optimization–guidelines, benchmarks and rules of thumb. Available from: https://europepmc.org/books/nbk326710
9. Cournia Z, Allen BK, Beuming T, Pearlman DA, Radak BK, Sherman W. Rigorous free energy simulations in virtual screening. J Chem Inf Model. 2020;60(9):4153–4169. doi:10.1021/acs.jcim.0c00116
10. Dougherty DA. The cation–π interaction. Acc Chem Res. 2013;46(4):885–893. doi:10.1021/ar300265y
11. Durrant JD, McCammon JA. Molecular dynamics simulations and drug discovery. BMC Biol. 2011;9:71. doi:10.1186/1741-7007-9-71
12. Ertl P, Rohde B, Selzer P. Fast calculation of molecular polar surface area as a sum of fragment-based contributions and its application to the prediction of drug transport properties. J Med Chem. 2000;43(20):3714–3717. doi:10.1021/jm000942e
13. Fan Z, Yao J, Li Y, Hu X, Shao H, Tian X. Anti-inflammatory and antioxidant effects of curcumin on acute lung injury in a rodent model of intestinal ischemia reperfusion by inhibiting the pathway of NF-κB. Int J Clin Exp Pathol. 2015;8(4):3451–3458.
14. Frauenfelder H, McMahon BH, Austin RH, Chu K, Groves JT. The role of structure, energy landscape, dynamics, and allostery in the enzymatic function of myoglobin. Proc Natl Acad Sci U S A. 2001;98(5):2370–2374. doi:10.1073/pnas.041614298
15. Gao F, Niu Y, Sun L, Li W, Xia H, Zhang Y, et al. Integrating network pharmacology and transcriptomic validation to investigate the efficacy and mechanism of Mufangji decoction preventing lung cancer. J Ethnopharmacol. 2022;298:115573. doi:10.1016/j.jep.2022.115573
16. Henzler-Wildman K, Kern D. Dynamic personalities of proteins. Nature. 2007;450(7172):964–972. doi:10.1038/nature06522
17. Hollingsworth SA, Dror RO. Molecular dynamics simulation for all. Neuron. 2018;99(6):1129–1143. doi:10.1016/j.neuron.2018.08.011
18. Jakowiecki J, Orzeł U, Chawananon S, Miszta P, Filipek S. The hydrophobic ligands entry and exit from the GPCR binding site—SMD and SuMD simulations. Molecules. 2020;25(8):1930. doi:10.3390/molecules25081930
19. Janin J, Bahadur RP, Chakrabarti P. Protein–protein interaction and quaternary structure. Q Rev Biophys. 2008;41(2):133–180.
20. Karplus M, McCammon JA. Molecular dynamics simulations of biomolecules. Nat Struct Biol. 2002;9(9):646–652. doi:10.1038/nsb0902-646
21. Kasuya Y, Kim JD, Hatano M, Tatsumi K, Matsuda S. Pathophysiological roles of stress-activated protein kinases in pulmonary fibrosis. Int J Mol Sci. 2021;22(11):6041. doi:10.3390/ijms22116041
22. Kinoshita T, Goto T. Molecular mechanisms of pulmonary fibrogenesis and its progression to lung cancer: A review. Int J Mol Sci. 2019;20(6):1461. doi:10.3390/ijms20061461
23. Kool J, Jonker N, Irth H, Niessen WMA. Studying protein–protein affinity and immobilized ligand–protein affinity interactions using MS-based methods. Anal Bioanal Chem. 2011;401(4):1109–1125. doi:10.1007/s00216-011-5207-9
24. Kumar PK, Awere CO, Kumari AR, Çolak AB, Bayrak M, Ogolla FO, et al. Machine learning-based identification of elite genotypes in the endangered Nilgirianthus ciliatus through qualitative and quantitative trait analysis. Curr Res Biotechnol. 2025;10:100307.

doi:10.1016/j.crbiot.2025.100307
25. Li ZH, Yu D, Huang NN, Wu JK, Du XW, Wang XJ. Immunoregulatory mechanism studies of ginseng leaves on lung cancer based on network pharmacology and molecular docking. Sci Rep. 2021;11(1):18201. doi:10.1038/s41598-021-97115-8
26. Limongelli V. Ligand binding free energy and kinetics calculation in 2020. Wiley Interdiscip Rev Comput Mol Sci. 2020;10(4):e1455. doi:10.1002/wcms.1455
27. Min TR, Park HJ, Ha KT, Chi GY, Choi YH, Park SH. Suppression of EGFR/STAT3 activity by lupeol contributes to the induction of apoptosis of human non-small cell lung cancer cells. Int J Oncol. 2019;55(1):320–330. doi:10.3892/ijo.2019.4799
28. Mobley DL, Dill KA. Binding of small-molecule ligands to proteins: "What you see" is not always "what you get." Structure. 2009;17(4):489–498. doi:10.1016/j.str.2009.02.010
29. Mohanty D, Padhee S, Priyadarshini A, Champati BB, Das PK, Jena S, et al. Elucidating the anti-cancer potential of Cinnamomum tamala essential oil against non-small cell lung cancer: A multifaceted approach involving GC–MS profiling, network pharmacology, and molecular dynamics simulations. Heliyon. 2024;10(6):e28026. doi:10.1016/j.heliyon.2024.e28026
30. Pedroza M, Le TT, Lewis K, Karmouty-Quintana H, To S, George AT, et al. STAT-3 contributes to pulmonary fibrosis through epithelial injury and fibroblast–myofibroblast differentiation. FASEB J. 2016;30(1):129–140. doi:10.1096/fj.15-273953
31. Rameshkumar R, Satish L, Pandian S, Rathinapriya P, Rency AS, Shanmugaraj G, et al. Production of squalene with promising antioxidant properties in callus cultures of Nilgirianthus ciliatus. Ind Crops Prod. 2018;126:357–367. doi:10.1016/j.indcrop.2018.10.031
32. Relas H, Gylling H, Miettinen TA. Fate of intravenously administered squalene and plant sterols in human subjects. J Lipid Res. 2001;42(6):988–994. doi:10.1016/S0022-2275(20)31623-0
33. Rout T, Mohapatra A, Kar M, Muduly DK. Essential protein identification in cancer: A graph-based approach integrating topological and biological features in PPI networks. SN Comput Sci. 2024;5(7):947. doi:10.1007/s42979-024-03312-3
34. Saleem S. Targeting MAPK signaling: A promising approach for treating inflammatory lung disease. Pathol Res Pract. 2024;254:155122. doi:10.1016/j.prp.2024.155122
35. Samarelli AV, Masciale V, Aramini B, Coló GP, Tonelli R, Marchioni A, et al. Molecular mechanisms and cellular contribution from lung fibrosis to lung cancer development. Int J Mol Sci. 2021;22(22):12179.
36. Sanders DJ, Minter HJ, Howes D, Hepburn PA. The safety evaluation of phytosterol esters. Part 6. The comparative absorption and tissue distribution of phytosterols in the rat. Food Chem Toxicol. 2000;38(6):485–491. doi:10.1016/S0278-6915(00)00021-1
37. Savin IA, Zenkova MA, Sen'kova AV. Pulmonary fibrosis as a result of acute lung inflammation: Molecular mechanisms, relevant in vivo models, prognostic and therapeutic approaches. Int J Mol Sci. 2022;23(23):14959. doi:10.3390/ijms232314959
38. Shi J, Chen J, Cheng C, Li W, Li M, Ye S, et al. Systems pharmacology-based drug discovery and active mechanism of Ganoderma lucidum triterpenoids for type 2 diabetes mellitus by integrating network pharmacology and molecular docking. Curr Pharm Des. 2025;31(33):2666–2690. doi:10.2174/0113816128365423250126035306
39. Sin ZW, Bhardwaj V, Pandey AK, Garg M. A brief overview of antitumoral actions of bruceine D. Explor Target Antitumor Ther. 2020;1(4):200. doi:10.37349/etat.2020.00013
40. Srinivasan M, Chandane AY, Tagalpallewar AA, Pawar AT, Nimbalkar M, Nimbalkar R, et al. Kerala's anticancer flora: A comprehensive review. J Appl Pharm Sci. 2024;14(9):018–045. doi:10.7324/JAPS.2024.180248
41. Tarbit MH, Berman J. High-throughput approaches for evaluating absorption, distribution, metabolism and excretion properties of lead compounds. Curr Opin Chem Biol. 1998;2(3):411–416. doi:10.1016/S1367-5931(98)80017-3
42. Tieyuan Z, Ying Z, Xinghua Z, Huimin W, Huagang L. Piceatannol-mediated JAK2/STAT3 signaling pathway inhibition contributes to the alleviation of oxidative injury and collagen synthesis during pulmonary fibrosis. Int Immunopharmacol. 2022;111:109107. doi:10.1016/j.intimp.2022.109107
43. Tran MT. Overview of Ca^{2+} signaling in lung cancer progression and metastatic lung cancer with bone metastasis. Explor Target Antitumor Ther. 2021;2(3):249. doi:10.37349/etat.2021.00045
44. Tuffery P, Derreumaux P. Flexibility and binding affinity in protein–ligand, protein–protein and multi-component protein interactions: Limitations of current computational approaches. J R Soc Interface. 2012;9(66):20–33. doi:10.1098/rsif.2011.0584
45. Tzouvelekis A, Gomatou G, Bouros E, Trigidou R, Tzilas V, Bouros D. Common pathogenic mechanisms between idiopathic pulmonary fibrosis and lung cancer. Chest. 2019;156(2):383–391. doi:10.1016/j.chest.2019.04.114
46. Vishveshwara S, Ghosh A, Hansia P. Intra and inter-molecular communications through protein structure

network. Curr Protein Pept Sci. 2009;10(2):146–160. doi:10.2174/138920309787847590

47. Wang W, Zheng F, Zhang A. Arsenic-induced lung inflammation and fibrosis in a rat model: Contribution of the HMGB1/RAGE, PI3K/AKT, and TGF-β1/SMAD pathways. Toxicol Appl Pharmacol. 2021;432:115757. doi:10.1016/j.taap.2021.115757

48. Yu W, Weng Y, Wang J, Gao Y, Li Y, Xie C, et al. Network pharmacology approach and partial experimental validation of Aidi injection solution for the treatment of colorectal cancer. Nat Prod Commun. 2024;19(3):1934578X241239169. doi:10.1177/1934578X241239169

49. Zhang Q, Liu J, Li R, Zhao R, Zhang M, Wei S, et al. A network pharmacology approach to investigate the anticancer mechanism and potential active ingredients of Rheum palmatum L. against lung cancer via induction of apoptosis. Front Pharmacol. 2020;11:528308. doi:10.3389/fphar.2020.528308

50. Zhang Y, Liang J, Cao N, Gao J, Song L, Tang X. Coal dust nanoparticles induced pulmonary fibrosis by promoting inflammation and epithelial–mesenchymal transition via the NF-κB/NLRP3 pathway driven by IGF1/ROS-mediated AKT/GSK3β signals. Cell Death Discov. 2022;8(1):500. doi:10.1038/s41420-022-01291-z

51. Zhou HX, Pang X. Electrostatic interactions in protein structure, folding, binding, and condensation. Chem Rev. 2018;118(4):1691–1741. doi:10.1021/acs.chemrev.7b00305

52. Zhou Y, Ling T, Shi W. Current state of signaling pathways associated with the pathogenesis of idiopathic pulmonary fibrosis. Respir Res. 2024;25(1):245. doi:10.1186/s12931-024-02878-z.

.